A simple explanation for the increase in relative humidity between 11 and 14 km in the tropics

Ian Folkins
Department of Physics and Atmospheric Science, Dalhousie University, Halifax, Nova Scotia, Canada

K. K. Kelly
National Oceanic and Atmospheric Administration, Aeronomy Laboratory, Boulder, Colorado, USA

E. M. Weinstock
Department of Chemistry and Chemical Biology, Harvard University, Cambridge, Massachusetts, USA

Received 7 February 2001; revised 23 June 2001; accepted 25 June 2002; published 14 December 2002.

[1] We use a very simple model with no adjustable parameters to simulate the increase in relative humidity between 11 and 14 km in the tropics. The rate of increase in relative humidity, in this interval, appears to be largely determined by the shape of the convective detrainment profile, the temperature profile, and the level of zero radiative heating. It appears to be unaffected by evaporative moistening or the complex three-dimensional structure of convective systems. We also show that the rapid increase in the fraction of supersaturated air parcels above 150 mb (~14.5 km) is associated with a transition from large scale descent to ascent. *INDEX TERMS:* 0322 Atmospheric Composition and Structure: Constituent sources and sinks; 0365 Atmospheric Composition and Structure: Troposphere—composition and chemistry; 0368 Atmospheric Composition and Structure: Troposphere—constituent transport and chemistry; *KEYWORDS:* Water vapor, tropical convection, relative humidity, upper troposphere

Citation: Folkins, I., K. K. Kelly, and E. M. Weinstock, A simple explanation for the increase in relative humidity between 11 and 14 km in the tropics, *J. Geophys. Res.*, *107*(D23), 4736, doi:10.1029/2002JD002185, 2002.

1. Introduction

[2] The mean tropical relative humidity profile is shaped like a "C", with large relative humidities in the boundary layer, a dry mid-troposphere, and large values again near the tropical tropopause [*Newell et al.*, 1997; *Jensen et al.*, 1999; *Vomel et al.*, 2002]. This profile is probably determined by some combination of subsidence drying, export of water vapor from the tropics to the extratropics [*Pierrehumbert*, 1998; *Zhu et al.*, 2000], moistening by convective detrainment and mixing, and the evaporation of water vapor from falling ice and water [*Sun and Lindzen*, 1993]. The relative magnitudes of these forcings are still, however, quite uncertain. The weaknesses in our current understanding of the water vapor budget limit our ability to predict how the earth's climate will respond to the increasing concentrations of carbon dioxide, since, although surface temperatures might be expected to continue to increase in response to higher levels of carbon dioxide, the magnitude of this increase will be strongly affected by the response of water vapor to these higher levels [*Manabe and Wetherald*, 1967].

[3] Figure 1 shows a compilation of relative humidity with respect to ice (RHI) measurements from three high altitude aircraft campaigns: the 1987 Stratospheric Tropospheric Exchange Project (STEP) [*Kelly et al.*, 1993], the 1993 Central Equatorial Pacific Experiment (CEPEX) [*Weinstock et al.*, 1995], and the 1994 Airborne Southern Hemisphere Ozone Experiment/Measurements for Assessing the Effects of Stratospheric Aircraft) (ASHOE/MAESA) [*Tuck et al.*, 1997]. Each relative humidity measurement represents a 10 second average, and comes from within the 20°S–20°N latitudinal band. Most of the STEP measurements were taken in the vicinity of Darwin in northern Australia, while most of the ASHOE/MAESA and CEPEX measurements occurred in the vicinity of Fiji. The water vapor measurements from the STEP and ASHOE/MAESA campaigns were obtained using the NOAA Aeronomy Laboratory Lyman α hygrometer, while those from the ER-2 during the CEPEX campaign were taken using the Harvard Lyman α hygrometer [*Weinstock et al.*, 1994]. A discussion of these instruments is given in the SPARC Assessment of Upper Tropospheric and Stratospheric Water Vapor [*Kley et al.*, 2000]. Temperature and pressure measurements from STEP and ASHOE/MAESA were made by the Micrometeorological Measurement System (MMS), which has a temperature accuracy at these altitudes of ±0.3 K, and a pressure accuracy of ±0.25 mb [*Chan et al.*, 1989]. Temperature and pressure measurements from the ER-2 during CEPEX were made using the NAV recorder, whose associated errors are likely to be larger than those from the MMS.

[4] The curve in Figure 1 with open boxes is an average of the relative humidity measurements in pressure intervals. Relative humidity measurements above 1.6 are occasionally present but have little impact on the average climatology. The mean relative humidity increases from about 0.5 below

0148-0227/02/2002JD002185$09.00

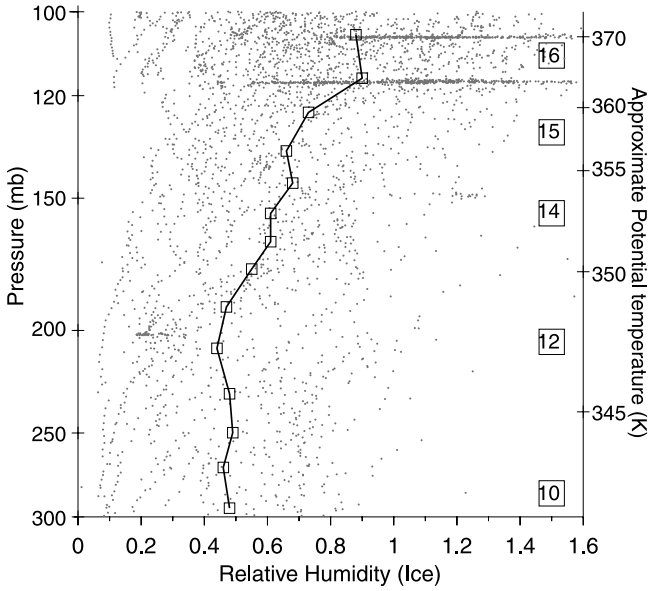

Figure 1. A compilation of all 10 sec averaged RHI measurements between 20°S and 20°N from the STEP, CEPEX, and ASHOE/MAESA aircraft campaigns. The solid line with open boxes represents a climatology (averaged in pressure intervals) from all three campaigns. Relative humidity measurements above 1.6 are not shown but are included in the climatology. Approximate heights are indicated by the boxes along the right hand axis.

200 mb to 0.7–0.9 above 150 mb. This paper addresses the reasons for this increase.

2. Model

[5] Figure 2 shows a simplified moisture budget of the upper tropical troposphere. The mean water vapor mixing ratio is assumed to equal a weighted average over air parcels which have detrained at various heights from deep convective clouds. Air parcels which detrain above the level of zero radiative heating (about 15 km) will be subject to mean ascent and are unlikely to influence the water vapor budget at lower altitudes. It is assumed that the water vapor mixing ratio of an air parcel at detrainment is equal to the saturation water vapor mixing ratio at that temperature, and that this mixing ratio is conserved during subsidence. This ignores possible increases in the water vapor mixing ratio due to evaporation of ice crystals falling from cirrus clouds at higher altitudes. The relative contribution of a given pressure interval to the weighted average is proportional to the detrainment rate at that pressure, $det(p)$, which can be thought of as the rate at which air at a given height is replaced by air brought up from the surface by deep convection. For example, a detrainment rate of 0.1 $(\text{days})^{-1}$ indicates that, on average, the air at that pressure is replaced once every ten days. With these assumptions, the mean water vapor mixing ratio at a pressure p is given by

$$[H_2O(p)] = \frac{\int_p^{p_{Q=0}} [H_2O_{sat}(p')] det(p') dp'}{\int_p^{p_{Q=0}} det(p') dp'}, \qquad (1)$$

where $p_{Q=0}$ is the pressure at which the clear sky radiative heating is zero, and $[H_2O_{sat}(p')]$ is the saturation water vapor mixing ratio corresponding to the temperature at pressure p'. In this model, the mean water vapor mixing ratio in the upper tropical troposphere is purely a function of the mean temperature and detrainment profiles, and the level of zero radiative heating. A detrainment profile which was sharply peaked near $p_{Q=0}$ would give rise to smaller mean water vapor mixing ratios than one in which deep convective outflow tended to occur at a lower altitude where the saturation water vapor mixing ratios at detrainment were larger.

[6] The dashed lines in Figure 3 show two relative humidity profiles generated by the model. The dashed line with the smaller relative humidity has been calculated using (1). The larger of the two dashed curves was also calculated from (1), but with the detrainment temperature increased by 1 K. The reasons for this shift will be discussed later. Between 11 and 14 km, the two curves agree reasonably well with the aircraft climatology (open boxes), and a climatology obtained from the Microwave Limb Sounder (MLS) [*Read et al.*, 2001]. The MLS climatology is an average of eight mean profiles, each from a different season, and from either the 20°S - Eq or Eq - 20°N latitude interval. The profiles are given from 6.5 km to 13.5 km in 1 km intervals, and have been converted to pressure using a climatological relationship between height and pressure. Also shown in Figure 3 is a relative humidity climatology compiled from approximately 800 sondes launched at nine different tropical locations as part of the SHADOZ project (Southern Hemisphere Additional Ozonesondes project [*Thompson et al.*, 2002]). Below the 0°C line (~600 mb),

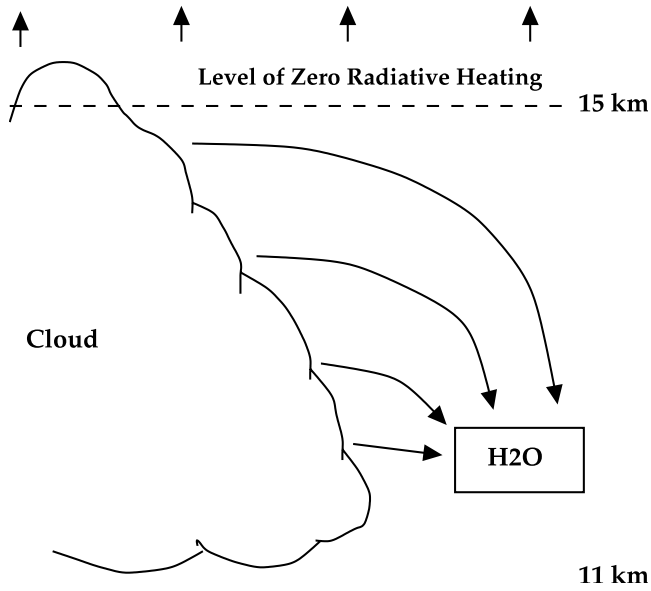

Figure 2. A picture of the simplified upper tropospheric moisture budget on which the model is based. The mean water vapor mixing ratio at a height between 11 and 15 km is assumed to arise from a weighted sum of all contributions between that height and the level of zero radiative heating. It is assumed that air parcels detrain with a water vapor mixing ratio equal to the local saturation value, and that this value is conserved during subsidence. The relative contribution of a given pressure interval to the mean water vapor mixing ratio is proportional to the detrainment rate at that pressure.

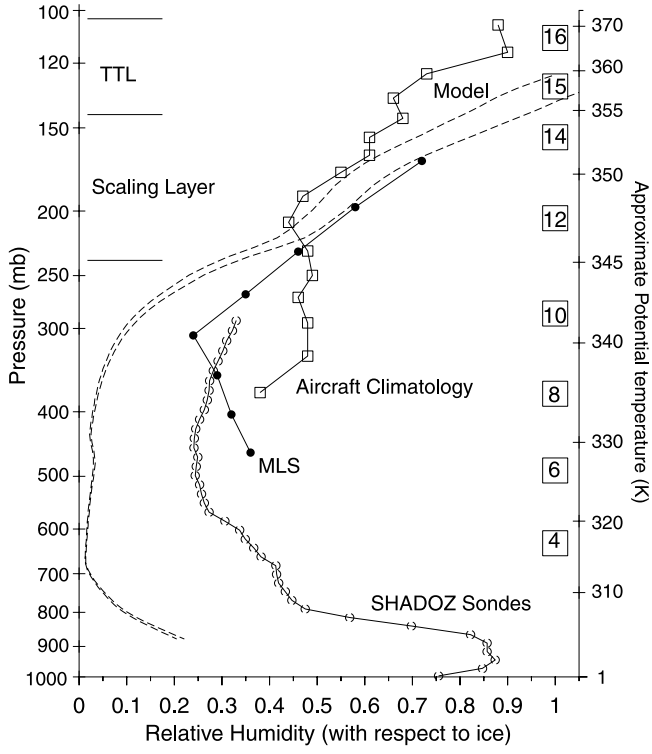

Figure 3. The curve with open circles is an RHI climatology compiled from about 800 high resolution radiosondes at nine different tropical SHADOZ locations. Data above 10 km (−35°C) is sometimes available but not shown because some humidity sensors exhibit a dry bias at cold temperatures. Below 600 mb, RHI has been converted to relative humidity with respect to water. The curve with open boxes is an upper tropospheric aircraft climatology obtained from the measurements shown in Figure 1. The curve with solid circles is an annual 20°S to 20°N MLS RHI climatology obtained from the MLS instrument [*Read et al.*, 2001]. The dashed curves are predictions of the mean tropical RHI profile obtained from a simple model. The larger of the two dashed curves is the result of a model run in which the detrainment temperature was increased by 1 K above the tropical mean temperature at that pressure. Approximate heights are given in the boxes along the right hand axis. The top of the convective boundary layer at 800 mb emerges as a strong feature in the SHADOZ climatology.

the relative humidity has been calculated with respect to the saturation vapor pressure of water rather than ice.

3. The Detrainment Profile

[7] The detrainment profile used in (1) is shown in Figure 4. It was determined from the tropical mean clear sky mass flux $M_r(p)$ using

$$det(p) = g\frac{dM_r(p)}{dp}. \quad (2)$$

The mass flux was determined from the clear sky heating rate $Q_r(p)$ using [*Minschwaner and McElroy*, 1992]

$$M_r(p) = \frac{\rho Q_r(p)}{dT/dz + \Gamma_d}, \quad (3)$$

where g is the gravitational acceleration, ρ the density, dT/dz the lapse rate, and Γ_d the dry adiabatic lapse rate. The clear sky radiative heating rate $Q_r(p)$ was calculated using a δ-four-stream radiative transfer code [*Fu and Liou*, 1992], with the input temperature, water vapor, and ozone profiles obtained from a compilation of radiosonde and satellite measurements [*Folkins*, 2002]. These input profiles were generated for each 5° latitude interval from 20°S to 20°N, and used to calculate heating rate and mass flux profiles within each interval. The mass flux profile, shown in Figure 5 was obtained by averaging over all mass flux profiles from 20°S to 20°N. This mass flux profile was then used in (2) to generate the detrainment profile shown in Figure 4.

[8] The use of (3) to estimate the downward mass flux in the tropics involves three main assumptions. First, it assumes that the area covered by slow radiatively driven subsidence is much larger than the area covered by cloud updrafts. This is probably a good assumption because most upward transport in the tropics occurs within deep convective clouds, which cover about 2.7% of the total area [*Rossow and Schiffer*, 1999]. Second, it assumes that the downward transport of mass associated with evaporative cooling from falling ice and rain can be ignored. This is a poor assumption in the mid and lower troposphere where the vertical mass fluxes associated with convective downdrafts are substantial, but it is probably a reasonable assumption in the upper troposphere. This is because, although falling ice crystals may evaporate and bring the

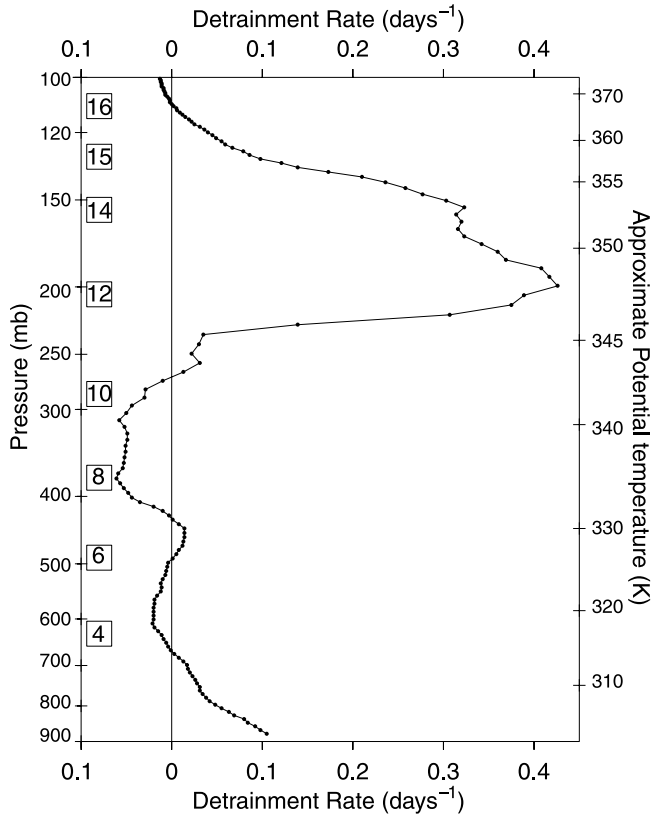

Figure 4. This figure shows the detrainment rate diagnosed from clear sky radiative heating. Deep convective detrainment occurs mainly between the 345 K and 365 K potential temperature surfaces (roughly 11 to 16 km).

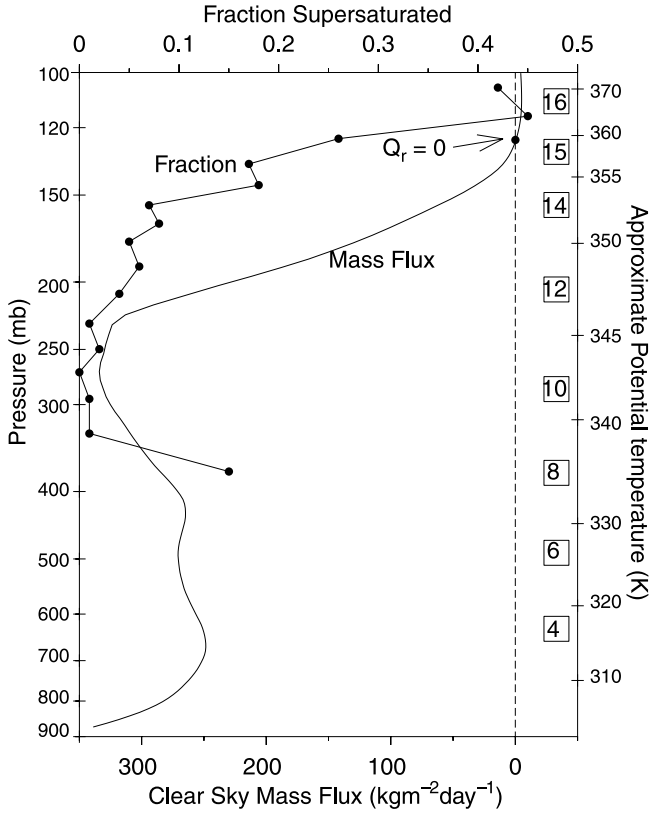

Figure 5. The solid curve is an estimate of the clear sky mass flux M_r in the tropics, based on temperature and mean trace gas profiles averaged from 20°S–20°N [*Folkins*, 2002]. The curve with closed circles represents the fraction of air parcels at each pressure which are supersaturated (RHI > 1). This fraction rapidly increases as the level of zero radiative heating is approached ($Q_r = 0$).

local atmosphere to saturation, temperatures in the upper tropical troposphere are sufficiently cold that the cooling associated with this evaporation should be too small to drive a significant downward mass flux. For example, the saturation water vapor mixing ratio at 230 mb (11 km) is about 175 ppmv, and the cooling associated with bringing an air parcel from a relative humidity of 0.5 to 1 is about 0.13 K. Given that clear sky radiative cooling rates at 230 mb are about 1.3 K/day, and that the fractional area covered by deep convective anvils at any one time is fairly small, it seems unlikely that the mass fluxes from evaporative cooling are comparable to those from radiative cooling at this height. Finally, (3) assumes that the effect of clouds on mean radiative heating rates is small. Although the instantaneous radiative heating rates from cloud top cooling and cloud base heating rates can be large, detailed calculations using realistic cloud distributions suggest that cloud radiative heating rates in the upper troposphere are significantly smaller than clear sky heating rates when averaged over the tropics as a whole [*Bergman and Hendon*, 1998].

[9] The use of (2) to infer convective detrainment in the upper tropical troposphere also involves several assumptions. In general, the difference in the vertical mass flux between two adjacent pressure levels in the tropics will be balanced by the sum of detrainment of mass into the layer by deep convective clouds, the entrainment of mass out of the layer by deep convection, and by the exchange of mass in that layer with higher latitudes. The entrainment of mass from a layer should be small if the mass fluxes associated with upper tropospheric convective downdrafts are small. Estimates of horizontal transport from radiosonde winds suggest that the exchange of mass with higher latitudes can be considered small in the 11 to 14 km interval where the vertical divergence is large [*Folkins*, 2002].

[10] Although the use of clear sky radiative heating rates to infer tropical mean detrainment rates is subject to a large number of assumptions, and can only be expected to be valid in the upper troposphere, some features of the inferred detrainment profiles are consistent with independent measurements. Lidar measurements from TOGA/COARE indicate that the mean base and top of deep convective anvil cirrus occur near 12 km and 16.85 km respectively [*Sassen et al.*, 2000]. Using a relationship between potential temperature and height, appropriate for this region and season, this height range corresponds to a potential temperature range of 348 K for cloud base to 368 K for cloud top [*Folkins*, 2002]. This is roughly the range over which the detrainment profile shown in Figure 4 is positive. It was also shown that, when implemented in a one-dimensional model, the detrainment profile shown in Figure 4 could be used to generate an ozone profile similar to observed climatologies [*Folkins et al.*, 2002].

[11] Figure 6 shows a compilation of 10 sec averaged ozone measurements from the STEP and ASHOE/MAESA aircraft campaigns. At marine tropical locations, such as Darwin (STEP) and Fiji (ASHOE/MAESA), ozone mixing ratios in the boundary layer (below 800 mb) are usually less than 20 ppbv. The highest potential temperature at which such low ozone values are found in the upper troposphere is 365 K. This suggests that the 365 K potential temperature surface is near the upper limit of moist undilute convective ascent from the boundary layer. This upper limit is consistent with Figure 4, which shows that the detrainment rate passes through zero near 365 K. One would also expect the rate of undilute convective detrainment to be small above 365 K because air parcels in the boundary layer with θ_e larger than 365 K are rarely observed [*Folkins*, 2002]. In most of the tropics, the 365 K potential temperature surface corresponds to an altitude of about 16 km. It corresponds to a somewhat higher altitude in regions such as the western tropical Pacific, where potential temperatures near the cold point tropopause tend to be displaced upward.

[12] The most remarkable feature of the detrainment profile shown in Figure 4 is the rapid increase near 230 mb (~11 km). A rapid increase in detrainment near this pressure has been previously inferred from an array of radiosonde profiles in the western tropical Pacific [*Yanai et al.*, 1973]. From a thermodynamic point of view, air parcels near the surface become able to participate in deep convection once their Convective Available Potential Energy (CAPE) is positive. In most of the tropics, the threshold pseudoequivalent potential temperature (θ_e) at which the CAPE of an air parcel becomes positive is near 345 K. If deep convective updrafts are able to transport nearly undilute boundary layer air into the upper tropical troposphere (so that the θ_e of these air parcels is conserved and they detrain near their level of neutral buoyancy), then one

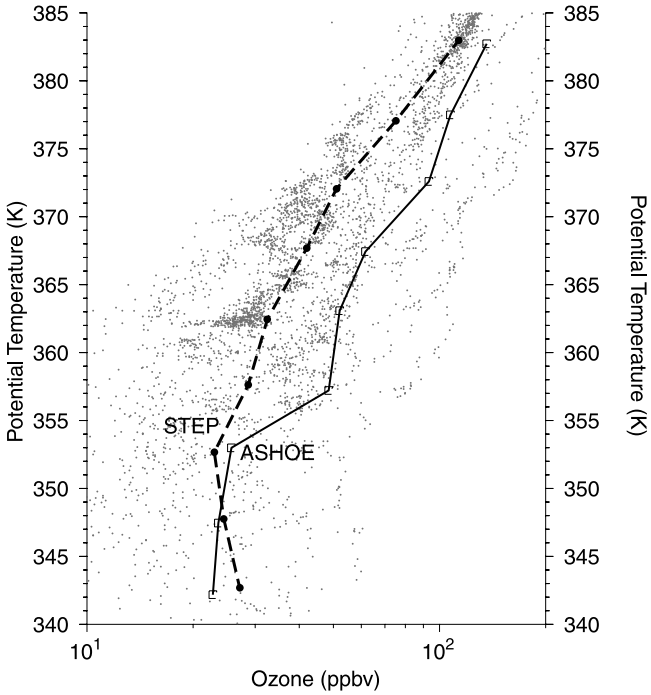

Figure 6. Ozone measurements from the STEP and ASHOE/MAESA aircraft campaigns (20°N–20°S) plotted against potential temperature. The dashed line is the STEP climatology, while the solid line with boxes is the ASHOE/MAESA climatology.

would expect the onset of deep convective detrainment to occur near the 345 K isentropic surface [*Folkins*, 2002].

4. Supersaturated Fraction

[13] Figure 1 shows that there is a greater abundance of supersaturated (RHI > 1) air parcels in the tropical troposphere at higher altitudes. In Figure 5, the fraction of supersaturated air parcels has been plotted as a function of pressure. This fraction rapidly increases above 150 mb (∼14.5 km) as the level of zero radiative heating is approached from below. Between the level of zero radiative heating and the cold point tropopause, large scale ascent will tend to increase the relative humidity, and, in the absence of ice condensation nuclei, will tend to generate relative humidities greater than one [*Jensen et al.*, 1999]. Below the level of zero radiative heating, large scale descent can be expected to significantly reduce the frequency of supersaturated air parcels.

5. Undulation of Potential Temperature Surfaces

[14] The temperatures used to calculate the relative humidities shown in Figure 1 are given in Figure 7. Superimposed on the STEP, ASHOE/MAESA, and CEPEX temperature measurements is a black line representing a 15°S–15°N annual climatology. Temperatures from STEP and ASHOE/MAESA exhibit a warm bias below 120 mb (∼15.3 km) and a cold bias above 120 mb. Temperatures from CEPEX were closer to the tropical mean. The most likely reason for the anomalous temperatures observed during these campaigns is

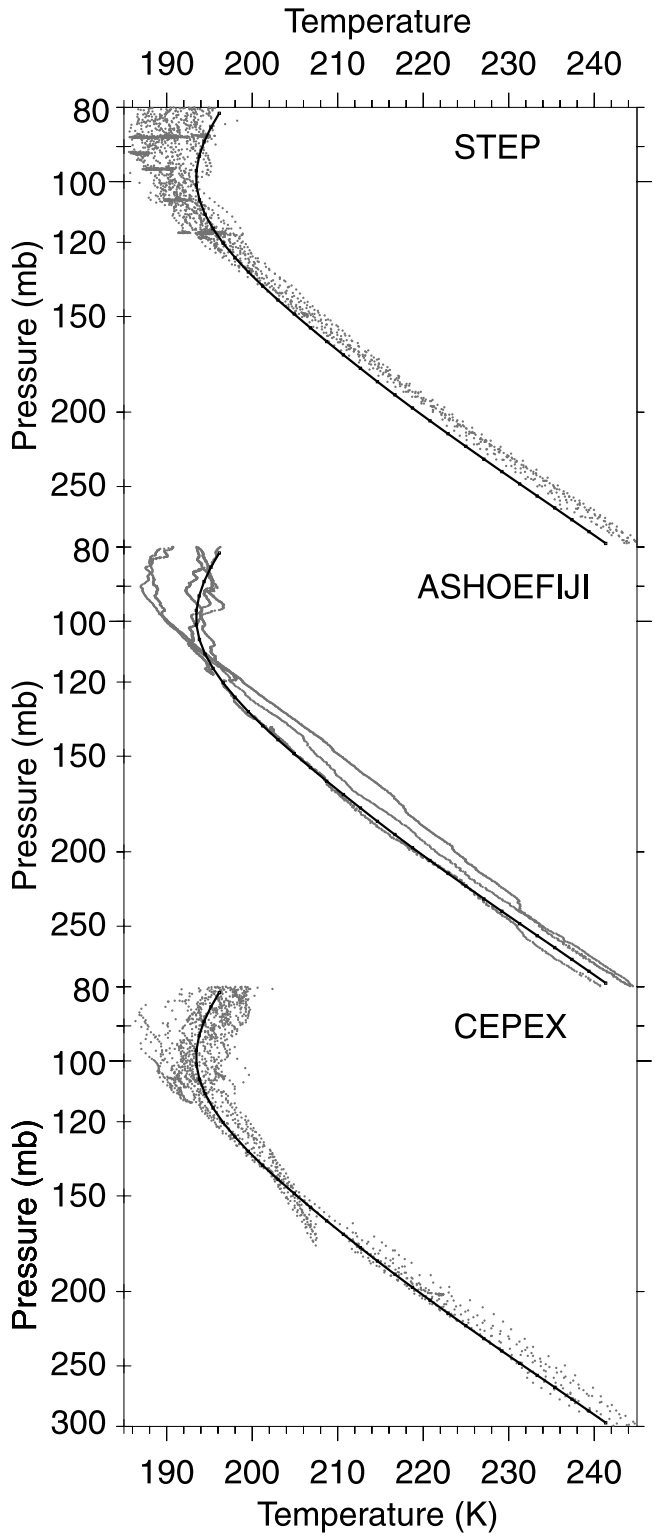

Figure 7. This figure shows the temperature measurements used to calculate the relative humidities given in Figure 1. In all three aircraft campaigns, but especially during STEP and ASHOE/MAESA, the temperature measurements below 120 mb exhibited a warm bias with respect to the mean annual tropical climatology, indicated by the solid line.

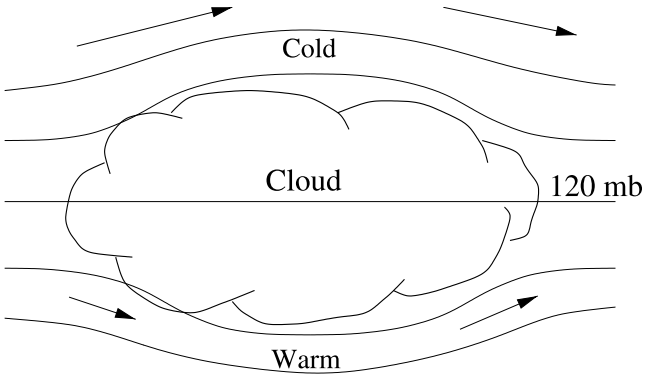

Figure 8. In the actively convective regions sampled by the STEP, ASHOE/MAESA, and CEPEX campaigns, temperatures tended to be warmer than the tropical mean below 120 mb, and colder than the tropical mean above 120 mb. This figure shows the impact such temperature perturbations would have on the shape of isentropic surfaces in these regions.

that they occurred in regions of active deep convection. In the case of STEP and ASHOE/MAESA, a likely contributing factor to the cold bias above 120 mb is that these measurements occurred during Northern Hemisphere winter. The pressure at which these temperature anomalies change sign ($\sim$120 mb) is quite close to the pressure at which clear sky radiative heating rates change sign ($\sim$125 mb), suggesting that convectively induced temperature anomalies are subject to radiative damping.

[15] The existence of temperature anomalies associated with tropical deep convection introduces ambiguities into the interpretation of relative humidity measurements obtained primarily from convective regions. The existence of a warm bias in convective regions would tend to reduce the relative humidity in these regions with respect to the tropical mean. This might explain why, as shown in Figure 3, the aircraft climatology is smaller than the MLS climatology between 12 and 14 km. On the other hand, this effect would be offset by a tendency for the relative humidity in convective regions to be larger than the tropical mean because air parcels in these regions have detrained more recently from convective clouds.

[16] If convective regions tend to be warmer than the tropical mean, then the use in (1) of a saturation water vapor mixing ratio at a detrainment temperature corresponding to the tropical mean at that pressure may be inappropriate. As a sensitivity test, we increased the detrainment temperature in (1) by 1 K. The resulting relative humidity profile is shown as the larger of the two dashed lines in Figure 3. Increasing the detrainment temperature by a constant shifts the modeled relative humidity profile, but has little effect on its slope.

[17] Figure 8 illustrates the effect of tropical deep convection on the shape of isentropic surfaces. As an air parcel below 120 mb enters a convective region, it will be adiabatically warmed as it moves along a downward sloping isentropic surface. This will tend to suppress the relative humidity in actively convecting regions. Air parcels leaving regions of active convection will experience an increase in relative humidity as they are adiabatically cooled along upward sloping isentropic surfaces, offset of course by subsidence warming associated with radiative cooling. The effects occur in reverse above 120 mb.

6. Discussion

[18] As shown in Figure 3, the modeled relative humidity profiles agree quite well with the observed climatologies between 11 and 14 km. This is coincident with the height range over which the detrainment rate appears to be controlled by the probability distribution function of θ_e in the convective boundary layer [*Folkins*, 2002]. It has been identified as the scaling layer in Figure 3. In the model, relative humidity increases with height in the scaling layer because the amount of post detrainment subsidence becomes progressively less as the level of zero radiative heating is approached from below. For example, the mean relative humidity at 11 km arises from an average over very moist air parcels which have recently detrained near 11 km and subsided very little, and very dry air parcels which have detrained near the level of zero radiative heating ($\sim$15.3 km) and subsided by more than 4 km. For air parcels at 15 km, however, the mean detrainment height can only be slightly larger than 15 km, so one would expect to observe a mean relative humidity only slightly less than 1. The good agreement between the model and the measurements in the rate at which relative humidity increases with height in the scaling layer provides some support that the detrainment profile shown in Figure 4 is realistic. For example, a detrainment profile weighted more strongly to a higher altitude would produce a relative humidity profile that had lower values at 11 km, and that increased with height more rapidly than observed.

[19] Also identified in Figure 3 is the Tropical Tropopause Layer (TTL) [*Highwood and Hoskins*, 1998; *Folkins et al.*, 1999]. This layer can be defined as the interval over which the mean temperature profile is controlled by both the Hadley and Brewer Dobson Circulations [*Folkins*, 2002]. The presence of large scale ascent in most of the TTL renders the model inapplicable in this region.

[20] Figure 3 shows that the modeled relative humidity is much lower than the observed climatologies below 11 km, so that the model is clearly inapplicable in this region also. Below 11 km, there is virtually no detrainment in the model, so that the modelled vapor mixing ratio is essentially equal to the mass weighted average of air parcels that have detrained in the scaling layer ($\sim$100 ppmv). This generates unrealistically low relative humidities in most of the tropical troposphere. This is presumably due to the absence from the model of processes such as shallow convection, evaporation of falling water and ice, and mixing along the sides of deep convective updrafts, which prevent relative humidities from approaching near zero values in the mid-troposphere. It should be noted, however, that the absence of these processes does not produce a relative humidity profile corresponding to the saturation water vapor mixing ratio of the tropical tropopause, as is sometimes thought. This would only occur if convective detrainment could be described as a δ function spike at the tropical tropopause.

[21] It is clear from (1) that the multiplication of the detrainment profile by a constant, with no change in tropical temperatures or the level of zero radiative heating, has no effect on the relative humidity profile generated by the model.

This suggests that a change in the intensity of the Hadley circulation should, by itself, have little effect on the mean relative humidity profile of the upper tropical troposphere.

[22] There have been several recent demonstrations that the observed relative humidity field in various parts of the tropics can be well simulated by large-scale advection, with the restriction that water vapor be at or below saturation [*Sherwood*, 1996; *Salathe and Hartmann*, 1997; *Pierrehumbert and Roca*, 1998; *Gettelman et al.*, 2000]. In particular, it has been shown, on the 215 and 146 mb surfaces, that the MLS relative humidity measurements can be reproduced by a three-dimensional model using realistic large scale winds, and a relative humidity cutoff of 1, but with no attempt to incorporate cloud microphysical processes [*Dessler and Sherwood*, 2000]. The success of this approach, in the language of this paper, may have arisen from the fact that both pressure surfaces lie within the scaling layer.

[23] Within a convective system, one would expect the evaporation of falling ice and water to increase the relative humidity of unsaturated air below the cirrus anvils, but not in the detraining air itself, since this air should be already close to saturation. The mean cloud base of deep convective cirrus anvils, at least in the western Pacific, is near 12 km [*Sassen et al.*, 2000]. This may help account for the absence of a need for an evaporative moisture source between 11 km and 14 km in the tropics.

7. Summary

[24] The water vapor budget of the tropical troposphere is very complicated, with fundamental quantities such as the mean precipitation efficiency still poorly constrained by measurements. We have shown, however, that for some portion of the upper tropical troposphere - the interval from 11 to 14 km - the mean relative humidity profile is determined by the deep convective detrainment profile, the temperature profile, and the height of the level of zero radiative heating.

[25] **Acknowledgments.** I. F. acknowledge many useful conversations with Andrew Dessler; he, in turn, acknowledges useful conversations with Richard Rood. I. F. thanks the National Center for Atmospheric Research for hosting a visit to the Atmospheric Chemistry Division where much of this research was done. Radiosonde date were provided through the SHADOZ database archived by J. C. Witte (SMAC at NASA-Goddard): http://code916.gsfc.nasa.gov/Data_services/shadoz. We thank M. Proffitt for ozone data from STEP and ASHOE/MAESA.

References

Bergman, J. W., and H. H. Hendon, Calculating monthly radiative fluxes and heating rates from monthly cloud observations, *J. Atmos. Sci.*, *55*, 3471–3491, 1998.

Chan, K. R., et al., Temperature and horizontal wind measurements on the ER-2 aircraft during the 1987 Airborne Antarctic Ozone Experiment, *J. Geophys. Res.*, *94*, 11,573–11,587, 1989.

Dessler, A. E., and S. C. Sherwood, Simulations of tropical upper tropospheric humidity, *J. Geophys. Res.*, *105*, 20,155–20,163, 2000.

Folkins, I., Origin of lapse rate changes in the upper tropical troposphere, *J. Atmos. Sci.*, *59*, 992–1005, 2002.

Folkins, I., M. Loewenstein, J. Podolske, S. Oltmans, and M. Proffitt, A barrier to vertical mixing at 14 km in the tropics: Evidence from ozonesondes and aircraft measurements, *J. Geophys. Res.*, *104*, 22,095–22,101, 1999.

Folkins, I., C. Braun, A. M. Thompson, and J. Witte, Tropical ozone as an indicator of deep convection, *J. Geophys. Res.*, *107*(D13), 4184, doi:10.1029/2001JD001178, 2002.

Fu, Q., and K. N. Liou, On the correlated k-distribution method for radiative transfer in nonhomogeneous atmospheres, *J. Atmos. Sci.*, *49*, 2139–2156, 1992.

Gettelman, A., J. R. Holton, and A. R. Douglass, Simulations of water vapor in the lower stratosphere and upper troposphere, *J. Geophys. Res.*, *105*, 9003–9023, 2000.

Highwood, E. J., and B. J. Hoskins, The tropical tropopause, *Q. J. R. Meteorol. Soc.*, *124*, 1579–1604, 1998.

Holton, J. R., and A. Gettelman, Horizontal transport and the dehydration of the stratosphere, *Geophys. Res. Lett.*, *28*, 2799–2802, 2001.

Jensen, E. J., et al., High humidities and subvisible cirrus near the tropical tropopause, *Geophys. Res. Lett.*, *26*, 2347–2350, 1999.

Kelly, K. K., et al., Water Vapor and cloud water measurements over Darwin during the STEP 1987 tropical mission, *J. Geophys. Res.*, *98*, 8713–8723, 1993.

Kley, D., J. M. Russell III, C. Phillips (Eds.), *SPARC Assessment of Upper Tropospheric and Stratospheric Water Vapour*, rep. 113, World Clim. Res. Programme (WCRP), Geneva, Switzerland, December 2000.

Manabe, S., and R. T. Wetherald, Thermal equilibrium of the atmosphere with a given distribution of relative humidity, *J. Atmos. Sci.*, *24*, 241–259, 1967.

Minschwaner, K., and M. B. McElroy, Radiative constraints on the energy budget of the tropical atmosphere, *Planet. Space Sci.*, *40*, 1585–1597, 1992.

Newell, R. E., Y. Zhu, W. G. Read, and J. W. Waters, Relationship between tropical upper tropospheric moisture and eastern tropical Pacific sea surface temperature at seasonal and interannual time scales, *Geophys. Res. Lett.*, *24*, 25–28, 1997.

Pierrehumbert, R. T., Lateral mixing as a source of subtropical water vapor, *Geophys. Res. Lett.*, *25*, 151–154, 1998.

Pierrehumbert, R. T., and R. Roca, Evidence for control of Atlantic subtropical humidity by large scale advection, *Geophys. Res. Lett.*, *25*, 4537–4540, 1998.

Read, W. G., J. W. Waters, D. L. Wu, E. M. Stone, and Z. Shippony, UARS Microwave Limb Sounder upper tropospheric humidity measurement: Method and validation, *J. Geophys. Res.*, *106*, 32,207–32,358, 2001.

Rossow, W. B., and R. A. Schiffer, Advances in understanding clouds from ISCCP, *Bull. Am. Meteorol. Soc.*, *80*, 2261–2287, 1999.

Salathe, E. P., and D. L. Hartmann, A trajectory analysis of tropical upper-tropospheric moisture and convection, *J. Clim.*, *10*, 2533–2547, 1997.

Sassen, K., R. P. Benson, and J. D. Spinhirne, Tropical cirrus cloud properties derived from TOGA/COARE airborne polarization lidar, *Geophys. Res. Lett.*, *27*, 673–677, 2000.

Sherwood, S. C., Maintenance of the free-tropospheric tropical water vapor distribution, part II, Simulation by large scale advection, *J. Clim.*, *9*, 2919–2934, 1996.

Sun, D., and R. Lindzen, Distribution of tropical tropospheric water vapor, *J. Atmos. Sci.*, *50*, 1643–1660, 1993.

Thompson, A. M., et al., The 1998–2000 SHADOZ (Southern Hemisphere Additional Ozonesondes) Tropical Ozone Climatology: Comparisons with TOMS and Ground-based Measurements, *J. Geophys. Res.*, in press, 2002.

Tuck, A. F., et al., The Brewer Dobson circulation in the light of high altitude in situ aircraft observations, *Q. J. R. Meteorol. Soc.*, *124*, 1–70, 1997.

Vömel, H., et al., Balloon-borne observations of water vapor and ozone in the tropical upper troposphere and lower stratosphere, *J. Geophys. Res.*, *107*, 4210, doi:10.1029/2001JD000707, 2002.

Weinstock, E. M., E. J. Hintsa, A. E. Dessler, J. F. Oliver, N. L. Hazen, J. N. Demusz, N. T. Allen, L. B. Lapson, and J. G. Anderson, New fast response photofragment fluorescence hygrometer for use on the NASA ER-2 and the Perseus remotely piloted aircraft, *Rev. Sci. Instrum.*, *65*, 3544–3554, 1994.

Weinstock, E. M., E. J. Hintsa, A. E. Dessler, and J. G. Anderson, Measurements of water vapor in the tropical lower stratosphere during the CEPEX campaign: Results and interpretation, *Geophys. Res. Lett.*, *22*, 3231–3234, 1995.

Yanai, M., S. Esbensen, and J. Chu, Determination of bulk properties of tropical cloud clusters from large-scale heat and moisture budgets, *J. Atmos. Sci.*, *30*, 611–627, 1973.

Zhu, Y., R. E. Newell, and W. G. Read, Factors controlling upper-troposphere water vapor, *J. Clim.*, *13*, 836–848, 2000.

I. Folkins, Department of Physics and Atmospheric Science, Dalhousie University, Halifax, Nova Scotia, Canada B3H 3J5. (Ian.Folkins@dal.ca)

K. K. Kelly, National Oceanic and Atmospheric Administration, Aeronomy Laboratory, R/AL2, 325 Broadway, Boulder, CO 80305-3328, USA. (kenneth.k.kelly@noaa.gov)

E. Weinstock, Department of Chemistry and Biological Chemistry, Harvard University, 12 Oxford Street, Cambridge, MA 02138, USA. (lliot@huarp.harvard.edu)